VOL. 13, NO. 1, JANUARY 2018 ISSN 1819-6608
ARPN Journal of Engineering and Applied Sciences

www.arpnjournals.com

UNSTEADY ALIGNED MHD BOUNDARY LAYER FLOW AND HEAT TRANSFER OF MAGNETIC NANOFLUID PAST A VERTICAL FLAT PLATE WITH LEADING EDGE ACCRETION

Mohd Rijal Ilias[1, 2], Noraihan Afiqah Rawi[2], Nurul Hidayah Ab Raji[1] and Sharidan Shafie[2]
[1]Department of Mathematical Sciences, Faculty of Computer and Mathematical Sciences, Universiti Teknologi MARA, Malaysia
[2]Department of Mathematical Sciences, Faculty of Science, Universiti Teknologi Malaysia, Johor Bahru, Malaysia
E-Mail: rijal_rs@hotmail.com

ABSTRACT

A theoretical study has been done for the unsteady aligned MHD boundary layer flow as well as magnetic nanofluid's heat transfer through a vertical flat plate with leading edge accretion. For conventional base fluid, water and kerosene been used as they contain magnetite (Fe_3O_4) nanoparticles. Magnetic (Fe_3O_4) and non-magnetic (Al_2O_3) nanoparticles are compared as well. The governing partial differential equations are reduced into nonlinear ordinary differential equations through a suitable similarity transformation, where the Keller box method is used to solve numerically. Graphical and tabular results are discussed quantitatively in terms of the impact of pertinent parameters like magnetic parameter, M, magnetic field inclination angle, α, nanoparticles volume fraction, ϕ and thermal buoyancy parameter, λ_T ,on the dimensionless velocity, skin friction coefficient, temperature and heat transfer rate. The outcomes indicate that the leading edge accretion can significantly alter the fluid motion and the heat transfer attributes.

Keywords: unsteady aligned MHD, vertical flat plate, magnetic nanofluids, leading edge accretion, volume fraction.

1. INTRODUCTION

The uneven nature of an extensive gamut of fluid flows has garnered significant attention. Most of the applications have an ideal flow environment surrounding the device that is nominally steady; however, sometimes undesirable unsteady effects could occur either due to non-uniformities or fluctuations in the surrounding fluid or due to self-induction in the body [1]. The study of unsteady boundary layers is based on the fact that all boundary layers in practice are, in a way, unsteady. Extensive study has been done on unsteady flows of non-Newtonian and viscous fluids. Researchers in fluid mechanics are now familiar with all the characteristic features associated with the unsteady effects. The principal ideas and significant contributions on the topic have been briefly reviewed by [2-8]. A better comprehension of uneven fluid flows and the utilisation of this know-how for new design approaches should offer considerable enhancements in performance, dependability, and costs of several fluid dynamic mechanisms.

A new class of fluid is the nanofluids containing nanometre-sized particles that are suspended in a base fluid. Fluids such as ethylene glycol, water and engine oil all have poor heat transfer properties like low thermal conductivity, which are considered crucial for heat transfer coefficient between the heat transfer surface and the heat transfer medium. Several experiments have confirmed nanofluids to possess significantly higher thermal conductivity when compared with the base fluids. Choi and Eastman [9] first termed "nanofluid" and discovered that in the base fluid, suspended nanoparticles can improve thermal conductivity significantly. Normally, nanoparticles are made up of SiC, Al_2O_3, AlN, TiO, Cu and graphite, and they possess high thermal conductivity than that of conventional base fluids. Eastman et al. [10] further discovered that the adding copper (10 nm) particles in ethylene glycol led to almost 40% increase in the thermal conductivity. Later, many other researchers [11-13] also reported that the thermal conductivity can be increased more by 20% by adding 1–5% nanoparticles by volume to ordinary heat transfer fluids.

In the presence of a magnetic field, when magnetic nanoparticles are added to the base fluids, ferrofluids tended to form a nanofluids subclass. Ferrofluids are also referred as magnetic nanofluids. They allow further manipulation of hydrodynamic and heat transfer characteristics since they respond to the applied magnetic fields [14]. Ferrofluids can be synthesised by employing different types of magnetic nanoparticles. However, aluminium oxide and magnetite (Fe_3O_4) nanoparticles are considered as the most suitable option due to their thermophysical properties and hence selected for the present work. Ferrofluids find frequent applications in a range of scientific fields. For example, numerous magnetic fluid-based scientific devices such as accelerometers, sensors, pressure transducers and densimeters make use of ferrofluids [15]. Even in the fields of biomedical engineering and biomedicine, ferrofluids have proved to be very useful in magnetically targeting the drug delivery to reach a specific region in the human body, in-vivo monitoring of brain's chemical activities, targeted destruction of tumours or cancer cells and removal of toxin from the human body for cancer treatment. In a medical treatment, the wide application of ferrofluids as magnetic nanoparticles is due to their capability to reach even the smallest capillaries of the body [16]. Another specific application of ferrofluids is in developing magnetic ink that is used for inexpensive,

high-speed and silent printers. In fluid dynamics, ferrofluids' potential application would be in the subsurface environmental engineering, where the flow of ferrofluids under the ground is controlled and directed through the use of externally applied magnetic fields [17-19].

The study involving the flow of electrically conducting fluids under a magnetic field is called magnetohydrodynamics (MHD). Based on several theoretical and experimental studies performed for conventional electrically conducting fluids, it has been suggested that transport and heat transfer characteristics are significantly influenced by the magnetic field. Recently, in metallurgy and the polymer industry, the application of MHD has gained significant attention of many researchers. Qasim *et al*. [20] investigated heat transfer in ferrofluid in the presence of applied magnetic field by taking a stretched cylinder that had uniform heat flux and slip condition bearing in mind the significance of magnetic field in nanofluids. They added magnetite (Fe_3O_4) and non-magnetic (Al_2O_3) nanoparticles to the conventional base fluid water and reported a comparative study. Qasim et al. [21] also explained the impacts of heat and mass diffusion on nanofluids studied in a moving permeable convective surface. Heat transfer with thermal radiation within an enclosure of semi annulus that was filled with ferrofluids was reported by Sheikholeslami and Ganji [22] by exposing it to a magnetic source. Sheikholeslami et al. [23-26] have presented numerous investigations related to ferrofluids and nanofluids. The effects of magnetic field on stagnation point problem of ferrofluids were investigated by Khan et al. [27] over a stretching sheet with viscous dissipation and heat transfer. For base fluids of water and kerosene oil, they considered three types of nanoparticles (magnetite (Fe_3O_4), cobalt ferrite ($CoFe_2O_4$) and Mn-Zn ferrite (Mn-$ZnFe_2O_4$)). An implicit finite difference scheme was employed along with the quasi-linearisation technique to determine numerical solutions for the governing problem. Khan et al. [28] studied the flow and heat transfer characteristics in ferrofluids over a flat plate that had uniform slip velocity and heat flux.

Todd [29] presented a new unsteady boundary layer problem that included the moving leading edge with a specific rate of accretion or ablation and Fang [30] did some additional analysis for the thermal boundary layers and momentum. This paper's goal acts as an extension to the study of Todd [29] and Fang [30] for a magnetic nanofluid's unsteady aligned MHD boundary layer. Moreover, comparison is made between non-magnetic (Al_2O_3) with magnetic (Fe_3O_4) nanoparticles.

2. MATHEMATICAL FORMULATION

Unsteady, two-dimensional laminar boundary layer flow of a nanofluid past a vertical plate has been considered. The unsteadiness is caused by the steady rate of accretion at the leading edge. Let U_∞ signify the uniform free stream velocity and T_∞ represent free stream temperature. The $x-$axis is taken vertically up towards the direction of free stream, while $y-$axis would be perpendicular to the free stream. To the flow, with acute angle, α, the aligned magnetic field is applied and it is expected to be a function of the distance from the origin denoted as $B(x) = B_o / \left((\cos\omega)\nu_f \tau + (\sin\omega)\left(\frac{\nu_f x}{U_\infty}\right)\right)^{1/2}$ with $B_o \neq 0$, where the coordinate along the plate is x. In all these studies, nanofluid is assumed to be incompressible, and the viscous dissipation, radiation and chemical reaction effects are neglected. Nanofluids are assumed to behave as single-phase fluids with local thermal equilibrium between the base fluid and the nanoparticles suspended in them so that no slip occurs between them. Water and kerosene-based nanofluid is the fluid here, which contains two different types of nanoparticles, i.e. alumina and magnetite. Table-1 presents the thermophysical properties. In all these studies, we assume that nanofluid is incompressible, and ignore the effects of viscous dissipation, radiation and chemical reaction. Nanofluids are expected to behave as single-phase fluids that can maintain local thermal equilibrium between the suspended nanoparticles and the base fluid so that no slip occurs between them. Figure-1 provides a schematic diagram of the problem.

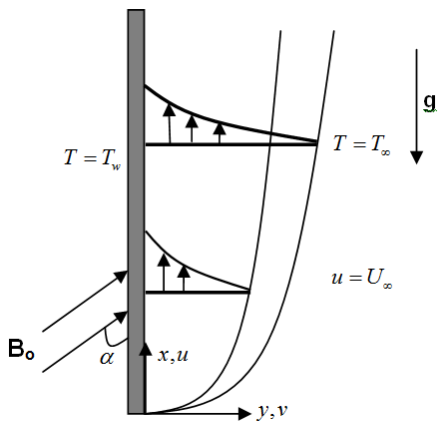

Figure-1. Flow configuration.

In all these studies, nanofluid is assumed to be incompressible, and the viscous dissipation, radiation and chemical reaction effects are neglected. Nanofluids are assumed to behave as single-phase fluids with local thermal equilibrium between the base fluid and the nanoparticles suspended in them so that no slip occurs between them.

$$\frac{\partial u}{\partial x} + \frac{\partial v}{\partial y} = 0 \tag{1}$$

$$\frac{\partial u}{\partial t}+u\frac{\partial u}{\partial x}+v\frac{\partial u}{\partial y}=\frac{\mu_{nf}}{\rho_{nf}}\frac{\partial^2 u}{\partial y^2}+\frac{(\rho\beta)_{nf}}{\rho_{nf}}g(T-T_\infty)-\frac{\sigma B^2(x)}{\rho_{nf}}\sin^2\alpha(u-U_\infty) \tag{2}$$

$$\frac{\partial T}{\partial t}+u\frac{\partial T}{\partial x}+v\frac{\partial T}{\partial y}=\alpha_{nf}\frac{\partial^2 T}{\partial y^2} \tag{3}$$

Boundary conditions of these equations are

$$\begin{aligned} &u=0,\quad v=0,\quad T=T_w \quad \text{at} \quad y=0,\\ &u\to U_\infty,\quad T\to T_w \quad \text{as} \quad y\to\infty. \end{aligned} \tag{4}$$

where u and v are velocity components in x and y directions, T is local temperature of nanofluid, g is acceleration due to gravity and σ is the electrical conductivity. Thermophysical properties of nanofluids, namely, ρ_{nf} is the effective density, μ_{nf} is the effective dynamic viscosity, $(\rho\beta)_{nf}$ is the thermal expansion coefficient and α_{nf} is the thermal diffusivity are given by

$$\rho_{nf}=(1-\phi)\rho_f+\phi\rho_s,\ \mu_{nf}=\frac{\mu_f}{(1-\phi)^{2.5}}$$
$$(\rho\beta)_{nf}=(1-\phi)(\rho\beta)_f+\phi(\rho\beta)_s,\ \alpha_{nf}=\frac{k_{nf}}{(\rho C_p)_{nf}}. \tag{5}$$

Here, ϕ is the solid volume fraction, μ_f is the dynamic viscosity of the base fluid, ρ_f and ρ_s are the densities of pure fluid and nanoparticles, respectively. $(\rho C_p)_{nf}$ is the heat capacity of the nanofluid and k_{nf} is the thermal conductivity of the nanofluid given by

$$(\rho C_p)_{nf}=(1-\phi)(\rho C_p)_f+\phi(\rho C_p)_s,$$
$$\frac{k_{nf}}{k_f}=\frac{k_s+2k_f-2\phi(k_f-k_s)}{k_s+2k_f+\phi(k_f-k_s)} \tag{6}$$

where $(\rho C_p)_f$ and $(\rho C_p)_s$ are the specific heat parameters of the base fluid and nanoparticles and k_f and k_s are thermal conductivities of the nanofluid and nanoparticles. The viscosity of the ferrofluid μ_{nf} can be approximated as the viscosity of a base fluid μ_f containing dilute suspension of fine spherical particles and is given by Brikmann [32]. The effective thermal conductivity of the nanofluid k_{nf} is approximated by Maxwell-Garnett's model, which is found to be appropriate for studying heat transfer enhancement using nanofluid.

Consider the following stream function as used in [29, 30, 33, 34]

$$\psi(x,y,t)=U_\infty\left((\cos\omega)\nu_f\tau+(\sin\omega)\left(\tfrac{\nu_f x}{U_\infty}\right)\right)^{1/2}f(\eta) \tag{7}$$

with the similarity variable (referred to as the Blasius–Rayleigh–Stokes variable in [29])

$$\eta=\frac{y}{\left((\cos\omega)\nu_f\tau+(\sin\omega)\left(\tfrac{\nu_f x}{U_\infty}\right)\right)^{1/2}} \tag{8}$$

and a nondimensional temperature $\theta=\theta(\eta)$ as

$$\theta(\eta)=\frac{T-T_\infty}{T_w-T_\infty} \tag{9}$$

where ω is unsteady parameter, ν_f is kinematic viscosity of fluid fraction and ψ is stream function which is defined in usual form as

$$u=\frac{\partial\psi}{\partial y}\quad\text{and}\quad v=-\frac{\partial\psi}{\partial x} \tag{10}$$

In terms of these new variables, the velocity components can be expressed as

$$u=U_\infty f'(\eta)$$
$$v=\left(\frac{\nu_f}{2}\right)\frac{(\eta f'-f)\sin\omega}{\left((\cos\omega)\nu_f\tau+(\sin\omega)\left(\tfrac{\nu_f x}{U_\infty}\right)\right)^{1/2}} \tag{11}$$

Using Eqns. (7) - (11) into Eqns. (1) - (4), the momentum and energy equations together with the boundary conditions can be written as

$$f'''+\frac{1}{2}(1-\phi)^{2.5}\left(1-\phi+\left(\frac{\phi\rho_s}{\rho_f}\right)\right)(\eta\cos\omega+f\sin\omega)f''+(1-\phi)^{2.5}M\sin^2\alpha(1-f')+(1-\phi)^{2.5}\left(1-\phi+\phi\frac{(\rho\beta)_s}{(\rho\beta)_f}\right)\lambda_T\theta=0 \tag{12}$$

$$\frac{k_{nf}}{k_f}\theta''+\frac{\Pr}{2}\left(\eta\cos\omega+f\sin\omega\right)\theta'=0 \tag{13}$$

with the boundary conditions

$$f(0)=0,\quad f'(0)=0,\quad \theta(0)=1,$$
$$f'(\eta)\to 1,\quad \theta(\eta)\to 0,\quad \text{as}\quad \eta\to\infty \tag{14}$$

Here the primes denote differentiations with respect to similarity variable η. The corresponding dimensionless group that appears in the governing equations are defined by: $\Pr=\nu_f/\alpha_f$ is the Prandtl number,

$$\lambda_T=\left(\left(\cos\omega\right)\nu_f\tau+\left(\sin\omega\right)\left(\tfrac{\nu_f x}{U_\infty}\right)\right)g\beta_f\left(T_w-T_\infty\right)/\nu_f U_\infty^{\,2}$$

is the free convection parameter [34], $M=\sigma B_o^{\,2}/\rho_f$ is the magnetic interaction parameter.

The quantities of physical interest in this work are the local Skin friction coefficient C_f and the local Nusselt number Nu_x are defined as

$$C_f=\frac{\tau_w}{\rho_f U_\infty^{\,2}}\quad\text{and}\quad Nu=\frac{xq_w}{k_f\left(T_w-T_\infty\right)} \tag{15}$$

where τ_w is the skin friction or the shear stress and q_w is the heat flux from the plate. τ_w and q_w are given by

$$\tau_w=\mu_{nf}\left(\frac{\partial u}{\partial y}\right)_{y=0}\quad\text{and}\quad q_w=-k_{nf}\left(\frac{\partial T}{\partial y}\right)_{y=0} \tag{16}$$

Substituting Eqns. (7) - (9) into Eqns. (15) and (16), the skin friction and reduced Nusselt number can be written as

$$\mathrm{Re}_x^{\,1/2}C_f=\frac{1}{\left(1-\phi\right)^{2.5}}\frac{f''(0)}{\left(\cos\omega\right)\tau+\sin\omega} \tag{17}$$

$$\mathrm{Re}_x^{\,-1/2}Nu=-\frac{k_{nf}}{k_f}\frac{\theta'(0)}{\left(\left(\cos\omega\right)\tau+\sin\omega\right)^{1/2}}$$

where $\mathrm{Re}_x=U_\infty x/\nu_f$ is the local Reynolds number and the nondimensional time variable $\tau=U_\infty t/x$ [35].

3. NUMERICAL SOLUTION

An efficient finite difference scheme called as Keller box method was employed for numerical calculation in the system of non-linear ordinary differential equations (12) and (13) along with the boundary condition (14). The employed scheme is a box method that was designed by Keller [36]. This method has proven to be accurate, especially for parabolic problems. This method offers faster rate, easy programming and more notably, it is the most flexible amongst common methods. It is preferred as it can easily adapt to solving equations regardless of any order. The Keller-box method is basically an implicit finite difference scheme and has proved itself to be very appropriate in dealing with nonlinear problems. Many recent publications may contain details of the method and, in this study; we have employed the procedure proposed in Cebeci and Pradshaw [37]. One of the basic ideas followed by the box method is to write in the form of a first order system for the governing system of equations. Therefore, the first derivatives of u, as well as other quantities with regards to η, need to be introduced as new unknown functions. Based on the resulting first order equations, we employ the "centred-difference" derivatives as well as averages at the net rectangles' midpoints and net segments, which are needed to achieve accurate finite difference equations. The resulting finite difference equations have found to be implicit and nonlinear in nature. The method of Newton is first introduced to linearize equations' nonlinear system prior to using a block-tridiagonal factorisation scheme on the finite difference equations' coefficient matrix. The block-elimination method solution can be employed to get the linearised system of difference equations [37]. In this study, we select a uniform grid with the size $\Delta\eta=0.01$ for meeting the convergence criteria of 10^{-7}, which offer almost six decimal places accuracy for almost all prescribed quantities.

4. RESULTS AND DISCUSSIONS

If the thermal buoyancy parameter is not present, $\lambda_T=0$, magnetic parameter, $M=0$, with no further addition of nanoparticles, $\phi=0$. The system of equations contains solutions that lie in the range of $-\frac{\pi}{4}\le\omega<\frac{3\pi}{4}$, which is comparable to the results achieved in [29, 30]. When $0<\omega\le\frac{\pi}{2}$, a leading edge accretion can be maintained with a rate of $U_\infty\cot\omega$, specifically the leading edge progressing upstream. When $\frac{\pi}{2}<\omega\le\omega_o$, where $\omega_o\approx 104.655°$ [30], a leading edge ablation occurs with a rate of $\left|U_\infty\cot\omega\right|$. When $-\frac{\pi}{4}\le\omega<0$, a "backward" boundary layer may be present with trailing edge accretion. At the critical points $\omega=0$ and $\omega=\frac{\pi}{2}$, the results can be seen similar to that of the well-known Rayleigh-Stokes problem and Blasius flat plate boundary layers, respectively. Blasius-Rayleigh-Stokes boundary layers are considered for all other solutions that lie in the range of $0<\omega<\frac{\pi}{2}$. Since the analytical solutions presented in Eqs. (5) and (6) are unavailable, the problem has to be solved by employing different numerical

techniques. For different parameters, the similarity equations have to be solved. The code was validated against the previous results prior to obtaining final results. To examine the behaviour of velocity and temperature profiles in terms of the physical problem, various values will carry numerical calculations, including magnetic interaction parameter, M, magnetic field inclination angle, α, thermal buoyancy parameter, λ_T and nanoparticles volume fraction, ϕ. For numerical computations, some of the non-dimensional values remain fixed, such as $\alpha = 90°, M = 2, \phi = 0.05$ and $\lambda_T = 1$. In the entire analysis, these values are treated to be common, excluding the different displayed values in specific tables and figures.

For different Pr values, Table-2 shows the comparison of $-\theta'(0)$ with by Bejan [39]. Moreover, Table-3 gives a list of the values of with those given by Todd [29] for different values of ω. Based on Table-3, it is seen that there is an increase in the skin friction coefficient with increasing ω. It is also observed that magnetic nanofluids have much more higher skin friction when compared with on-magnetic nanofluid and pure fluid. The comparisons are found to be in an excellent agreement as shown.

Table-1. Thermophysical properties of base fluids and ferroparticle [23, 28, 38].

Physical properties	Water	Kerosene	Fe_3O_4	Al_2O_3
$\rho(kg/m^3)$	997.1	780	5200	3970
$C_p(J/kgK)$	4179	2090	670	765
$k(W/mK)$	0.613	0.149	6	40
$\beta \times 10^{-5}(K^{-1})$	21	99	1.3	0.85
Pr	6.2	21		

Table-2. Comparison of $-\theta(0)$ values for different values of Pr when $\omega = \pi/2, \lambda_T = 0, M = 0, \phi = 0$ (pure fluid).

Pr	Bejan [39]	Present study
0.7	0.292	0.292683
0.8	0.307	0.306918
1	0.332	0.332059
5	0.585	0.576696
6.2 (water)	---	0.620077
10	0.730	0.728155
21(kerosene)	---	0.933538

The velocity and temperature distribution are presented in Figure-2 and Figure-3 for the entire flow of the Fe_3O_4–water nanofluid as well as the effect of α. With an increase in α for $\omega = 45°, 70°$ and $90°$, there is an increase in flow velocity and decrease in the boundary layer thickness (Figure-2).

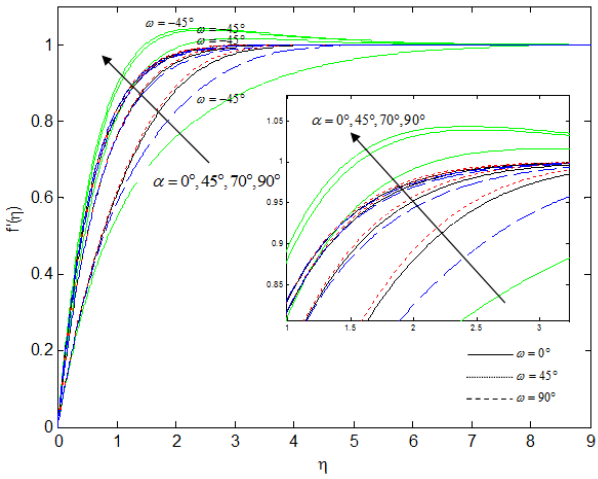

Figure-2. Effect of α on velocity for various ω.

As seen in Figure-3, there is a decrease in the temperature of the Fe_3O_4–water at a fixed point as well as the thermal boundary layer with rise in α for $\omega = 45°, 70°$ and $90°$. For $\omega = 0°$, there was no influence on the temperature due to variation of α. As mentioned in [29], $\omega = 0°$ corresponds to Rayleigh-Stokes layer where the problem is considered as a purely diffusive boundary layer that has complete absence of convection. On the other hand, there was increase in both temperature and thermal boundary layer when $\omega = -45°$, due to an increase in α. As highlighted in [29] and [30], an unsteady boundary layer of a trailing edge accretion could

occur when there is a negative value of ω. Mathematically, negative values of ω could also be presented; however, this flow did not find much practical applications and is not discussed here for other parameters.

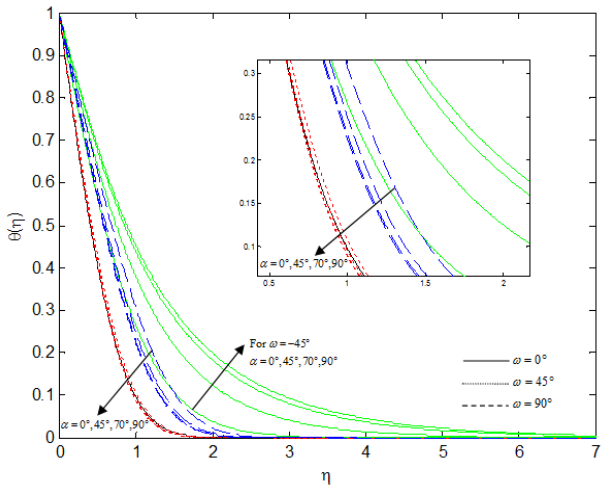

Figure-3. Effect of α on temperature for various ω.

Figure-4 and Figure-5 show the effect of M on the flow and temperature profiles for four different values. $M = 0$ occurs for condition when the applied magnetic field is missing. As M increases in Figure-4, velocity also gets accelerated in all cases of ω. It has been proven that the magnetic force allows enhancing the boundary layer as the term $(U_\infty - u)$ continues to remain positive in the momentum equation in the boundary layer region. On an increase in M, the Lorentz force associated with the boundary layer gets thinner for the magnetic field. The magnetic lines move based on the free stream velocity as they move past the plate. The magnetic field pushes the fluid that was decelerated due to viscous force, which also counteracts the viscous effects. Hence, with any increase in M for $\omega = 0°, 45°$ and $90°$., the velocity of the fluid also increases. Based on Figure-5, it is seen that the temperature decreases with increase in M in free stream conditions. A decrease in the thermal boundary layer thickness occurs with increase in M for $\omega = 45°$ and $90°$. For $\omega = 0°$, there was no change in the temperature.

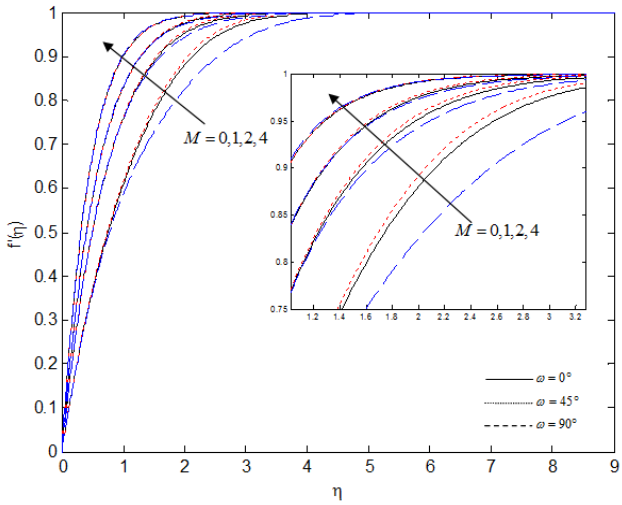

Figure-4. Effect of M on velocity for various ω.

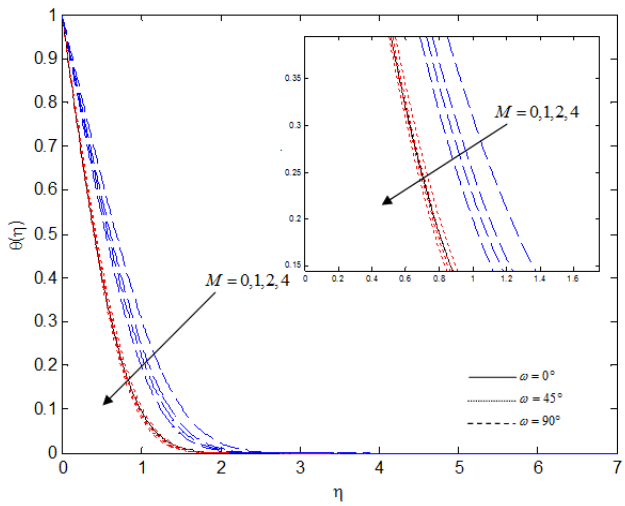

Figure-5. Effect of M on temperature for various ω.

Table-3. Comparison of $f''(0)$ values for different values of ω when $\omega = \pi/2, \lambda_T = 0, M = 0$.

Accretion rate (approximate)	ω	Pure fluid		Magnetic nanofluid $(\phi = 0.05)$		Non-Magnetic Nanofluid $(\phi = 0.05)$	
		Todd [29]	Present study	Fe_3O_4-water	Fe_3O_4-kerosene	Al_2O_3-water	Al_2O_3-kerosene
Rayleigh-Stokes	0	0.5642	0.564191	0.661912	0.681462	0.644832	0.660196
$(7.596)U_\infty$	$\frac{\pi}{24}$	0.5750	0.575018	0.673678	0.692736	0.657047	0.672006
$(3.732)U_\infty$	$\frac{\pi}{12}$	0.5807	0.580731	0.679485	0.697910	0.663424	0.677870
$(1.732)U_\infty$	$\frac{\pi}{6}$	0.5770	0.577004	0.673405	0.690109	0.658875	0.671943
U_∞	$\frac{\pi}{4}$	0.5529	0.552877	0.643446	0.657763	0.631020	0.642194
$(0.577)U_\infty$	$\frac{\pi}{3}$	0.5072	0.507220	0.588181	0.599310	0.578551	0.587209
$(0.268)U_\infty$	$\frac{5\pi}{12}$	0.4369	0.436866	0.503658	0.510452	0.497808	0.503067
$(0.132)U_\infty$	$\frac{11\pi}{24}$	0.3900	0.39000	0.447367	0.451264	0.444027	0.447029
Blasius	$\frac{\pi}{2}$	0.3321	0.332059	0.377490	0.377490	0.377490	0.377490

Increase in λ_T causes improving velocity of fluid enhances for $\omega = 0°, 45°$ and $90°$ (Figure-6). The reason behind this phenomenon could be λ_T, which is defined as the ratio of buoyancy to viscous forces in the boundary layer. Therefore, the fluid viscosity reduces with increase in its values, which in turn increases the flow velocity. In this Figure, $\lambda_T = 0$ indicates the absence of free convection, while $\lambda_T > 0$ gives rises to the cooling problem. On the other hand, the increase of λ_T is caused by the rise in buoyancy force. This force through convection enhances the heat transfer rate. The greater convection is caused by increase in temperature, which decreases the density of the nanofluid at higher temperature. It is clear that the fluid velocity possessing lesser density is greater when compared with larger density fluid. Figure-7 depicts the impact of λ_T on dimensionless temperature. It has been observed that the temperature decreases with increases in λ_T for $\omega = 0°, 45°$ and $90°$. It agrees with the fact that there is an increase in the fluid velocity due to buoyancy force, which could result in decrease in the temperature of the fluid to decrease. Also, we have noted down the decrease in thermal boundary layer thickness. For $\omega = 0°$, there was no change in the temperature.

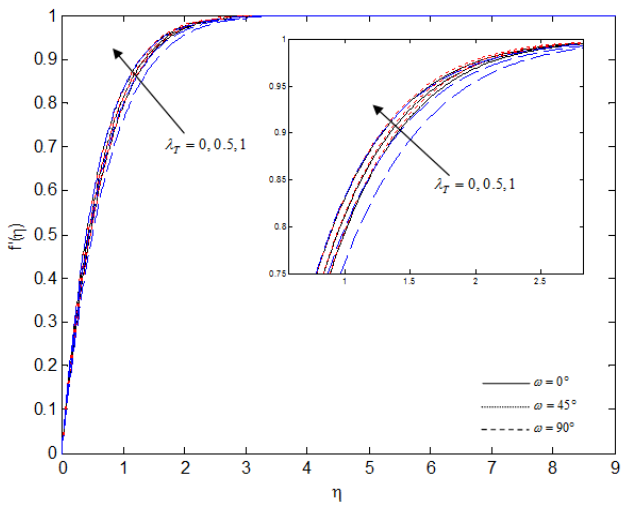

Figure-6. Effect of λ_T on velocity for various ω.

Figure-8 shows the effects of ϕ on the velocity of Fe_3O_4–water nanofluid. It has been proved that there is a decrease in velocity with increase in ϕ for $\omega = 0°, 45°$ and $90°$. Physically, this could be because of the reason that any increase in ϕ results in improving thermal conductivity. Hence, there is increase in thickness of the thermal boundary layer as well as for viscosity, and finally a decrease in velocity. According to Brickman and Maxwell [10] models, a nanofluid's viscosity and thermal conductivity increased with rise in volume fraction. This resulted in a decrease in nanofluid's velocity. For example, $\phi = 0$ corresponds to that of pure water.

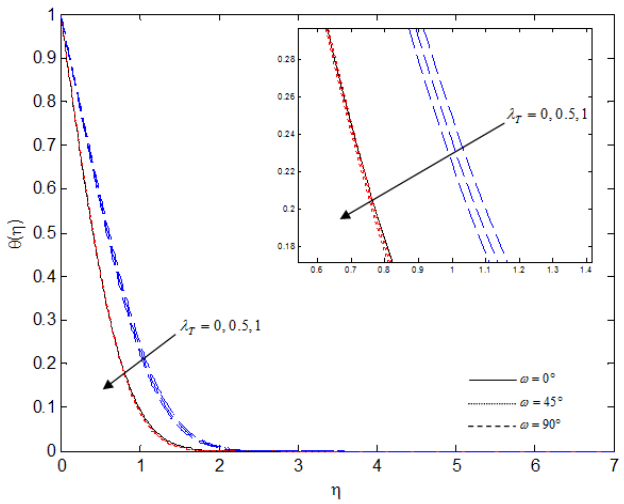

Figure-7. Effect of λ_T on temperature for various ω.

Figure-9 shows the effect of ϕ on the distribution of temperature. There is an increase in the fluid temperature as ϕ amplifies or $\omega = 0°, 45°$ and $90°$. Also, for Fe_3O_4–water nanofluid, the thermal boundary layer is greater compared with pure water, $\phi = 0$. This is due to the fact that magnetite possesses high thermal conductivity and adding it to the water-based fluid results in enhancing fluid's thermal conductivity, and so an increase in the thickness of the thermal boundary layer can be observed. It is also seen that the thermal boundary layer expands with increase in ϕ. This is in line with nanoparticles' physical behaviour. This observation signifies that employing Fe_3O_4–water nanofluids would be beneficial in the cooling and heating processes.

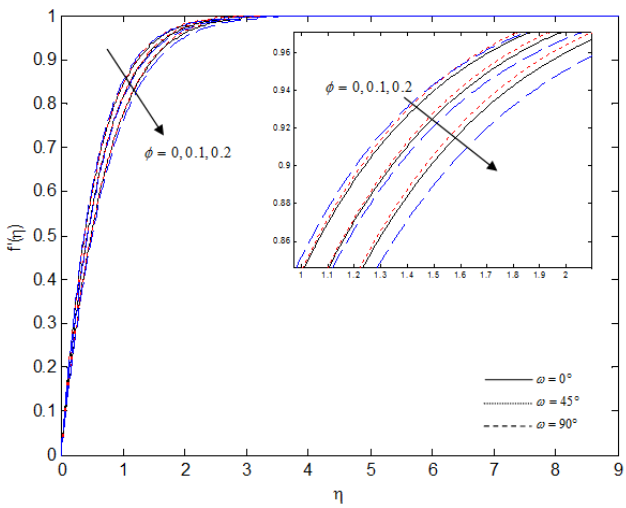

Figure-8. Effect of ϕ on velocity for various ω.

Figure-10 is plotted for the nanofluid (when the added nanoparticles include Al_2O_3) and the magnetic nanofluid (when the added nanoparticles include Fe_3O_4) and also when the volume fraction is $\phi = 0.05$. It was seen that the magnetic nanofluid's temperature was smaller compared with the nanofluid's temperature for all cases of ω. The magnetic nanofluid's viscosity and thermal conductivity are temperature dependent. Increase in temperature amplifies conductivity whilst increase in temperature leads to decrease in viscosity. Furthermore, the viscosity was found to be greater in Fe_3O_4 compared with Al_2O_3. This graphical observation was observed to be alike the experimental outcomes obtained by Colla [40].

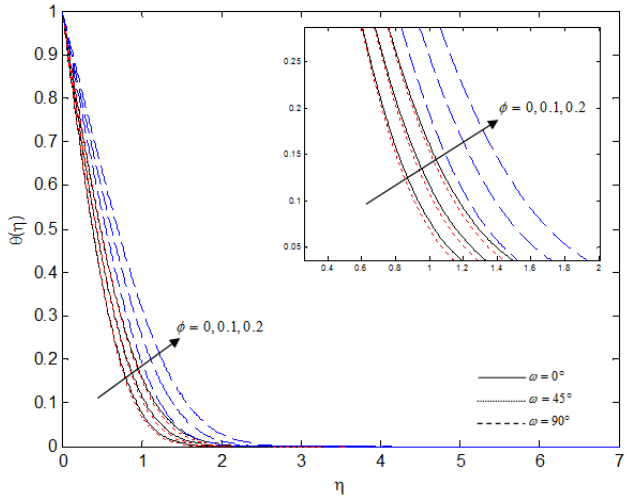

Figure-9. Effect of ϕ on temperature for various ω.

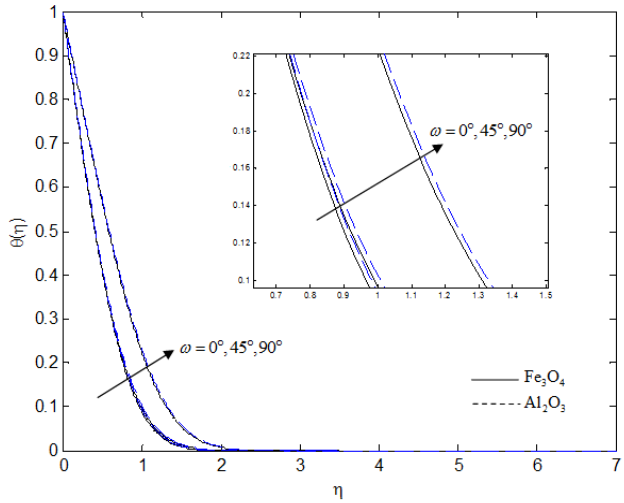

Figure-10. Comparison between magnetic (Fe_3O_4) and non-magnetic (Al_2O_3) nanoparticles.

Table-4. Variation in skin friction for magnetic nanofluids and non-magnetic nanofluids at different parameters.

α	M	λ_T	ϕ	Fe_3O_4-water (Fe_3O_4-kerosene)			Al_2O_3-water (Al_2O_3-kerosene)		
				0°	45°	90°	0°	45°	90°
0°	2	1	0.05	1.046877 0.900685	1.052346 0.901922	1.041075 0.851687	1.033976 0.881759	1.043987 0.889052	1.042158 0.853506
45°				1.562081 1.442421	1.558449 1.443476	1.559863 1.440777	1.555599 1.433344	1.553993 1.437419	1.559876 1.441847
70°				1.847057 1.740654	1.840990 1.740348	1.840867 1.741337	1.841898 1.733825	1.837363 1.735799	1.840621 1.742214
90°				1.924251 1.821156	1.917741 1.820510	1.917069 1.821841	1.919340 1.814796	1.914272 1.816252	1.916771 1.822675
90°	0	1	0.05	1.046877 0.900685	1.052346 0.901922	1.041075 0.851687	1.033976 0.881759	1.043987 0.889052	1.042158 0.853506
	1			1.562081 1.442421	1.558449 1.443476	1.559863 1.440777	1.555599 1.433344	1.553993 1.437419	1.559876 1.441847
	2			1.924251 1.821156	1.917741 1.820510	1.917069 1.821841	1.919340 1.814764	1.914272 1.816252	1.916771 1.822675
	4			2.476329 2.393516	2.468254 2.390957	2.463961 2.391930	2.472527 2.389117	2.465498 2.388029	2.463413 2.392536
90°	2	0	0.05	1.624683 1.631762	1.793182 1.622669	1.544888 1.544888	1.618667 1.624072	1.613343 1.617192	1.544888 1.544888
		0.5		1.774467 1.726459	1.768315 1.721829	1.733529 1.685034	1.769004 1.719418	1.764444 1.716966	1.733362 1.685458
		1.0		1.924251 1.821156	1.917741 1.820510	1.917069 1.821841	1.919340 1.814764	1.914272 1.816252	1.916771 1.822675
90°	2	1	0	1.796951 1.694572	1.793182 1.698534	1.806527 1.719801	1.796951 1.694572	1.739182 1.698534	1.806527 1.719801
			0.05	1.924251 1.821156	1.917741 1.820510	1.917069 1.821841	1.919340 1.814764	1.914272 1.816252	1.916771 1.822675
			0.10	2.066797 1.963686	2.057986 1.958536	2.041610 1.937261	2.055833 1.949677	2.050140 1.949104	2.040613 1.938773
			0.15	2.227611 2.125324	2.217249 2.116042	2.183230 2.069081	2.209335 2.102319	2.204038 2.100409	2.181141 2.071128
			0.20	2.410509 2.310068	2.399831 2.297441	2.345957 2.221249	2.383494 2.276476	2.380149 2.274435	2.342375 2.223694

Table-4 depicts the numerical denominations of $f''(0)$ for various values of α, M, λ_T and ϕ. The table also compares the magnetic and non-magnetic nanofluids. It is quite evident that the values of $f''(0)$ rise with α, M λ_T and ϕ for $\omega = 0°, 45°$ and $90°$. Furthermore, the ϕ propels the friction factor coefficients for each of the three cases. The nanofluids' density rises with a rise in ϕ. As a result, the skin friction rises as well. In case of $\omega = 0°$ and $45°$, the non-magnetic nanofluids friction factor coefficient is less when a comparison is done with magnetic nanofluids; however, it depictsa reverse behaviour in case of $\omega = 90°$.

Table-5 exhibits the variation in local Nusselt for various values of non-dimensional factors. The heat transfer rates are stimulated with enhancing values of α, M, λ_T and ϕ for $\omega = 45°$ and $90°$. In case of $\omega = 0°$, only ϕ enhances the transfer rate whereas others parameters do not cause any impact. The Nusselt numbers rise with rising ϕ. This is because of a rise in nanofluids' thermal conductivity with escalating ϕ. The transfer rate of heat is greater in non-magnetic nanofluids in comparison to magnetic nanofluids. As the magnetic field's strength is raised, the magnetic nanoparticles line up in one direction and demonstrate greater heat transfer rates that are analogous to non-magnetic nanoparticles.

Table-5. Variation in Nusselt number for magnetic nanofluids and non-magnetic nanofluids at different parameters.

α	M	λ_T	ϕ	Fe_3O_4-water (Fe_3O_4-kerosene)			Al_2O_3-water (Al_2O_3-kerosene)		
				0°	45°	90°	0°	45°	90°
0°	2	1	0.05	1.478101 2.845697	1.385383 2.542806	0.840060 1.255682	1.496604 2.839373	1.403506 2.536286	0.855565 1.258004
45°				1.478101 2.845697	1.427647 2.610570	0.940759 1.488219	1.496604 2.839373	1.447168 2.605587	0.957127 1.489878
70°				1.478101 2.845697	1.447012 2.642673	0.980142 1.572375	1.496604 2.839373	1.466987 2.638060	0.996886 1.573854
90°				1.478101 2.845697	1.451853 2.650826	0.989636 1.592503	1.496604 2.839373	1.471930 2.646287	1.006471 1.593939
90°	0	1	0.05	1.478101 2.845697	1.385383 2.542806	0.840060 1.255682	1.496604 2.839373	1.403506 2.536286	0.855565 1.258004
	1			1.478101 2.845697	1.427647 2.610570	0.940759 1.488219	1.496604 2.839373	1.447168 2.605587	0.957127 1.489878
	2			1.478101 2.845697	1.451853 2.650826	0.989636 1.592503	1.496604 2.839373	1.471930 2.646287	1.006471 1.593939
	4			1.478101 2.845697	1.482332 2.703471	1.047035 1.714070	1.496604 2.839373	1.502972 2.699276	1.064398 1.715235
90°	2	0	0.05	1.478101 2.845697	1.434463 2.635626	0.939308 1.532747	1.496604 2.839373	1.454069 2.630894	0.955272 1.533931
		0.5		1.478101 2.845697	1.443528 2.643273	0.965424 1.563525	1.496604 2.839373	1.463102 2.638639	0.981837 1.564841
		1.0		1.478101 2.845697	1.451853 2.650826	0.989636 1.592503	1.496604 2.839373	1.471930 2.646287	1.006471 1.593939
90°	2	1	0	1.404848 2.585611	1.379410 2.410536	0.942332 1.457862	1.404848 2.858611	1.379410 2.410536	0.942332 1.457862
			0.05	1.478101 2.845697	1.451853 2.650826	0.989636 1.592503	1.496604 2.839373	1.471930 2.464287	1.006471 1.593939
			0.10	1.552537 3.119794	1.524857 2.902918	1.036383 1.730989	1.590132 3.106940	1.565704 2.893723	1.070648 1.734226
			0.15	1.628552 3.409808	1.598734 3.168392	1.082738 1.873956	1.686252 3.390550	1.661481 3.154764	1.135360 1.879614
			0.20	1.706559 3.717965	1.673806 3.449099	1.128874 2.022161	1.785846 3.692810	1.760064 3.431642	1.201148 2.031156

5. CONCLUSIONS

The present study investigates the numerical solution of unsteady aligned MHD flow of magnetic nanofluids over a vertical flat plate with leading edge accretion. The non-linear governing partial differential equations are transformed using suitable transformations and solved numerically by finite difference scheme. Physically, the effect of magnetic interaction parameter, M, magnetic field inclination angle, α, thermal buoyancy parameter, λ_T and nanoparticles volume fraction, ϕ were studied in detail and the results are discussed graphically and tabular. The main findings of this study can be summarized as follows:

- Velocity increases as α, M and λ_T increase for $\omega = 0°, 45°$ and $90°$.
- Velocity decreases with the increase in ϕ for $\omega = 0°, 45°$ and $90°$.
- Temperature increases with the increase in ϕ for $\omega = 0°, 45°$ and $90°$.
- Temperature decreases with the increase in α, M and λ_T for $\omega = 45°$ and $90°$, while unchanged for $\omega = 0$.
- Local skin friction increases with the increase in α, M λ_T and ϕ for $\omega = 0°, 45°$ and $90°$.
- Reduced Nusselt number increases with the increase in α, M and λ_T for $\omega = 45°$ and $90°$, while unchanged for $\omega = 0$.
- Reduced Nusselt number increases with the increase in ϕ for $\omega = 0°, 45°$ and $90°$.

REFERENCES

[1] McCroskey W. J. 1977. Some current research in unsteady fluid dynamics. ASME J. Fluids Eng. 99(1): 8-39.

[2] Stewartson K. 1960. The theory of unsteady laminar boundary layers. Advances in Applied Mechanics, 6, 1-37.

[3] Stuart J. T. 1963. Unsteady boundary layers. Laminar boundary layers. 349-408.

[4] Riley N. 1975. Unsteady laminar boundary layers. SIAM review. 17(2): 274-297.

[5] Riley N. 1990. Unsteady viscous flows. Science Progress. (1933): 361-377.

[6] Telionis D. P. & Telionis D. P. 1981. Unsteady viscous flows (Vol. 9). New York: Springer Verlag.

[7] Wang C. Y. 1989. Exact solutions of the unsteady Navier-Stokes equations. Appl. Mech. Rev. 42(11), 269-282.

[8] Pop I. & Ingham D. B. 2001. Convective heat transfer: mathematical and computational modelling of viscous fluids and porous media. Elsevier.

[9] Chol S. U. S. 1995. Enhancing thermal conductivity of fluids with nanoparticles. ASME-Publications-Fed. 231, 99-106.

[10] Eastman J. A., Choi S. U. S., Li S., Yu W. & Thompson L. J. 2001. Anomalously increased effective thermal conductivities of ethylene glycol-based nanofluids containing copper nanoparticles. Applied physics letters. 78(6): 718-720.

[11] Li Q., Xuan Y. & Wang J. 2003. Investigation on convective heat transfer and flow features of nanofluids. Journal of Heat transfer. 125: 151-155.

[12] Xue Qing-Zhong. 2003. Model for effective thermal conductivity of nanofluids. Physics letters A. 307.5: 313-317.

[13] Maiga S. E. B., Palm S. J., Nguyen C. T., Roy G. & Galanis N. 2005. Heat transfer enhancement by using nanofluids in forced convection flows. International journal of heat and fluid flow. 26(4): 530-546.

[14] Khan W. A., Makinde O. D. & Khan Z. H. 2014. MHD boundary layer flow of a nanofluid containing gyrotactic microorganisms past a vertical plate with Navier slip. International Journal of Heat and Mass Transfer. 74, 285-291.

[15] Parekh K. & Lee H. S. 2012, June. Experimental investigation of thermal conductivity of magnetic nanofluids. In: AIP Conference Proceedings. 1447(1): 385-386. AIP.

[16] Andablo-Reyes E., Hidalgo-Álvarez R., & de Vicente J. 2011. Controlling friction using magnetic nanofluids. Soft Matter. 7(3): 880-883.

[17] Chiang Y. C., Chieh J. J. & Ho C. C. 2012. The magnetic-nanofluid heat pipe with superior thermal properties through magnetic enhancement. Nanoscale research letters. 7(1): 322.

[18] Patel R. 2012. Effective viscosity of magnetic nanofluids through capillaries. Physical Review E. 85(2): 026316.

[19] Olanrewaju A. M. & Makinde O. D. 2013. On boundary layer stagnation point flow of a nanofluid over a permeable flat surface with Newtonian heating. Chemical Engineering Communications. 200(6): 836-852.

[20] Qasim M., Khan Z. H., Khan W. A. & Shah I. A. 2014. MHD boundary layer slip flow and heat transfer of ferrofluid along a stretching cylinder with prescribed heat flux. PloS one. 9(1): e83930.

[21] Qasim M., Khan I. & Shafie S. 2013. Heat transfer and mass diffusion in nanofluids over a moving permeable convective surface. Mathematical Problems in Engineering.

[22] Sheikholeslami M. & Ganji D. D. 2014. Ferrohydrodynamic and magnetohydrodynamic effects on ferrofluid flow and convective heat transfer. Energy. 75, 400-410.

[23] Sheikholeslami M., Ganji D. D. & Rashidi M. M. 2015. Ferrofluid flow and heat transfer in a semi annulus enclosure in the presence of magnetic source considering thermal radiation. Journal of the Taiwan Institute of Chemical Engineers. 47, 6-17.

[24] Sheikholeslami M., Bandpy M. G., Ellahi R. & Zeeshan A. 2014. Simulation of MHD CuO–water

nanofluid flow and convective heat transfer considering Lorentz forces. Journal of Magnetism and Magnetic Materials. 369, 69-80.

[25] Sheikholeslami M., Gorji-Bandpy M. & Ganji D. D. 2014. MHD free convection in an eccentric semi-annulus filled with nanofluid. Journal of the Taiwan Institute of Chemical Engineers. 45(4): 1204-1216.

[26] Sheikholeslami M., Gorji-Bandpy M., Ganji D. D. & Soleimani S. 2014. Natural convection heat transfer in a nanofluid filled inclined L-shaped enclosure. Iranian Journal of Science and Technology. Transactions of Mechanical Engineering. 38(M1+): 217.

[27] Khan Z. H., Khan, W. A., Qasim M. & Shah I. A. 2014. MHD stagnation point ferrofluid flow and heat transfer toward a stretching sheet. IEEE Transactions on Nanotechnology. 13(1): 35-40.

[28] Ram P. & Kumar V. 2014. Swirling Flow of Field Dependent Viscous Ferrofluid Over a Porous Rotating Disk with Heat Transfer. International Journal of Applied Mechanics. 6(04): 1450033.

[29] Todd L. 1997. A family of laminar boundary layers along a semi-infinite flat plate. Fluid dynamics research. 19(4): 235-249.

[30] Fang T. 2008. A note on the unsteady boundary layers over a flat plate. International Journal of Non-Linear Mechanics. 43(9): 1007-1011.

[31] Tiwari R. K. & Das M. K. 2007. Heat transfer augmentation in a two-sided lid-driven differentially heated square cavity utilizing nanofluids. International Journal of Heat and Mass Transfer. 50(9): 2002-2018.

[32] Brinkman H. C. 1952. The viscosity of concentrated suspensions and solutions. The Journal of Chemical Physics. 20(4): 571-571.

[33] Fang T., Zhang J., & Yao S. 2010. A new family of unsteady boundary layers over a stretching surface. Applied Mathematics and Computation. 217(8): 3747-3755.

[34] Van Gorder R. A. & Vajravelu K. 2009. Unsteady boundary layers: convective heat transfer over a vertical flat plate. The ANZIAM Journal. 50(4): 541-549.

[35] Stewartson K. 1973. On the impulsive motion of a flat plate in a viscous fluid. II. The Quarterly Journal of Mechanics and Applied Mathematics. 26(2): 143-152.

[36] Keller H. B. 1971. A new difference scheme for parabolic problems, Numerical solutions of partial differential equations. Academic Press, New York.

[37] Cebeci T. & Bradshaw P. 2012. Physical and computational aspects of convective heat transfer. Springer Science & Business Media.

[38] Oztop H. F. & Abu-Nada E. 2008. Numerical study of natural convection in partially heated rectangular enclosures filled with nanofluids. International journal of heat and fluid flow. 29(5): 1326-1336.

[39] Bejan A. 2013. Convection heat transfer. John wiley & sons.

[40] Colla L., Fedele L., Scattolini M. & Bobbo S. 2012. Water-based Fe_2O_3 nanofluid characterization: thermal conductivity and viscosity measurements and correlation. Advances in Mechanical Engineering. 4, 674947.